Rate-dependent behaviour of clay during cyclic 1D compression

Comportement visqueux des argiles en compression oedométrique

S. Kawabe
Tokyo University of Science, Japan
W. Kongkitkul
King Mongkut's University of Technology Thonburi, Thailand
D. Hirakawa
National Defence Academy of Japan, Japan
F. Tatsuoka
Tokyo University of Science, Japan

ABSTRACT

Drained constant-rate-of-strain one-dimensional compression tests at different strain rates with and without large unload/reload cycles and many sustained loading (SL) stages, as well as standard consolidation tests, were performed on reconstituted and undisturbed soft clays. Significantly rate-dependent stress-strain behaviour of *Isotach* type, not due to delayed dissipation of excessive pore water pressure but due to the viscous properties of clay, was observed. The creep axial strain rate at SL stages while otherwise the effective axial stress σ'_a was increasing at positive axial strain rates $\dot{\varepsilon}_a$ was always positive. The creep axial strain rate at SL stages while otherwise σ'_a was decreasing was basically negative, whereas it was positive immediately after load reversal from primary loading. Irrespective of the signs of current $\dot{\sigma}'_a$ and $\dot{\varepsilon}_a$, primary loading and reloading are defined by $\dot{\varepsilon}_a^{ir} > 0$, while unloading by $\dot{\varepsilon}_a^{ir} < 0$. These trends of behaviour are simulated by the non-linear three-component elasto-viscoplastic model.

RÉSUMÉ

Des essais oedométriques à vitesse de déformation constante avec ou sans cycles de charge/décharge et périodes de fluages, ainsi que des essais oedométriques standards (application de paliers de contrainte) ont été réalisés sur des échantillons prélevés peu perturbés et sur des échantillons remaniés d'argile. Le comportement observé est de type Isotach, dû aux propriétés visqueuses des argiles. Il a été vérifié que ce comportement n'est pas dû à la dissipation éventuelle de surpressions interstitielles. La vitesse de déformation irréversible (ou visco-plastique) observée lors des périodes successives de fluages atteintes après augmentation de la contrainte axiale est toujours positive, le reste juste après inversion du chargement puis devient négative lors des phases de fluage appliquées après diminution supplémentaire de la contrainte. Les phases de charge et de recharge sont définies par une vitesse de déformation irréversible positive tandis que la phase de décharge est définie par une vitesse de déformation irréversible négative. Les différents essais ont pu être correctement simulés par un modèle rhéologique élasto-visco-plastique non-linéaire à trois composantes.

Keywords: Clay, Creep, Loading/unloading/reloading, One-dimensional compression, Three-component model, Viscous property

1 INTRODUCTION

Most previous studies on long-term residual settlement of soft clay deposits focused on the behaviour during primary loading under mechanically normal consolidation (NC) conditions associated with, for example, fill construction and pumping of ground water. This behaviour is due to not only delayed dissipation of excess pore water pressure but also the viscous property of clay (e.g. Adachi et al. 1996). Under one-dimensional (1D) NC conditions, the viscous property of soft clay is generally *Isotach* type in that the current effective stress is a unique function of instantaneous irreversible strain and its rate irrespective of previous loading history (e.g., Imai 1995; Niemunis & Krieg 1996; Leroueil et al. 1996; Tanaka 2005a, b).

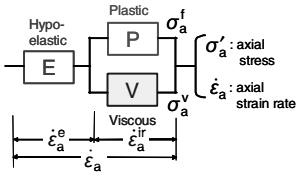

Fig. 1 Non-linear three-component model (Di Benedetto et al., 2002; Tatsuoka et al., 2002; Tatsuoka et al., 2008) applied to 1D compression

On the other hand, study on this topic under general loading conditions where the effective stress increases or decreases arbitrarily (e.g. continuously, multiple-stepwise, cyclically) and corresponding constitutive modelling is very limited (e.g., Acosta-Martínez et al. 2005). In this study, a series of 1D compression tests on reconstituted and undisturbed soft clays were performed at different strain rates under general loading conditions. The experimental results were simulated by a non-linear three-component elasto-viscoplastic model (Fig. 1).

Table 1. Test cases reported in this paper

Test No.	Clay type	Liquid limit, w_L, %	Plasticity index, PI	Initial water content, w_0, %	Initial void ratio, e_0
1	Fujinomori (reconstituted)	46.0	23.3	41.9	1.125
2				42.3	1.126
3				42.8	1.165
4				42.1	1.131
5				42.5	1.153
6				44.3	1.196
7		43.6	20.0	42.8	1.165
8				42.3	1.134
9	Yokohama (undisturbed)	83.6	44.0	66.2	1.835
10				72.5	1.968

2 TEST METHOD

Table 1 lists the test cases reported in this paper. The reconstituted specimens of Fujinomori clay were produced by consolidating slurry prepared at a water content two times of the liquid limit at σ_a = 100 kPa in a large cylinder. A large clay cake was cut to test specimens (6 cm in diameter & 2 cm-high). A number of undisturbed samples retrieved from a Holocene

doi:10.3233/978-1-60750-031-5-303

soft clay deposit in Yokohama city were also tested. In tests 1 – 7 & 9, the specimens were set in a newly designed oedometer (Fig. 2) with the top and bottom ends drained and loaded by using an automated pneumatic loading system. In tests 8 & 10, the specimen bottom end was undrained with pore water pressure measurement and axial loading was strain-controlled by using a precision-gear system. Nearly full drainage in these tests was confirmed. To eliminate possible variance among the data of tests 1 – 4, the specimens were recompressed to σ'_a = 100 kPa by monotonic loading (ML) at $\dot{\varepsilon}_a$ = 0.05 %/min, followed by sustained loading (SL) for one day, unloading to σ'_a = 5 kPa and final SL for one day. In Fig. 3a, the origin: ε_a = 0 is defined at the end of this SL stage.

As seen from Figs. 3, 4 & 5, the following loading schemes were employed: 1) the standard consolidation test (SCT) with multiple step increases in the axial stress, σ_a , at a ratio $\Delta\sigma_a/\sigma_a$ = 1.0 every 24 hours; 2) constant-rate-of-strain (CRS)

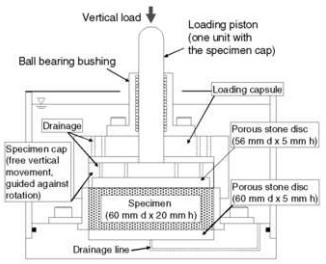

Fig. 2 Oedometer used in the present study

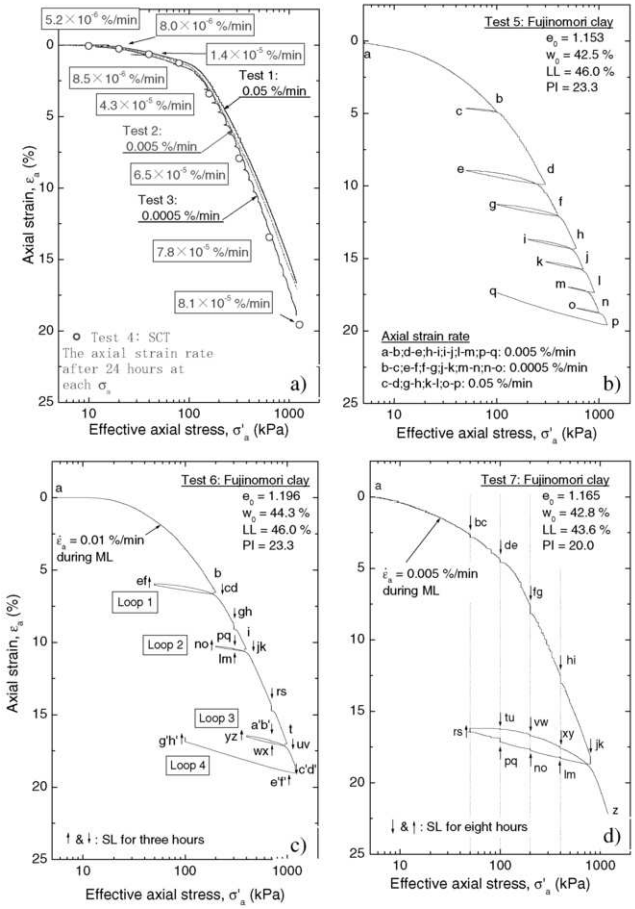

Fig. 3 a) ML tests 1, 2 & 3 at different constant $\dot{\varepsilon}_a$ s and a SCT; b) ML test at different $\dot{\varepsilon}_a$ s in different loading segments; and c) & d) SL during primary loading, unloading and reloading, Fujinomori clay

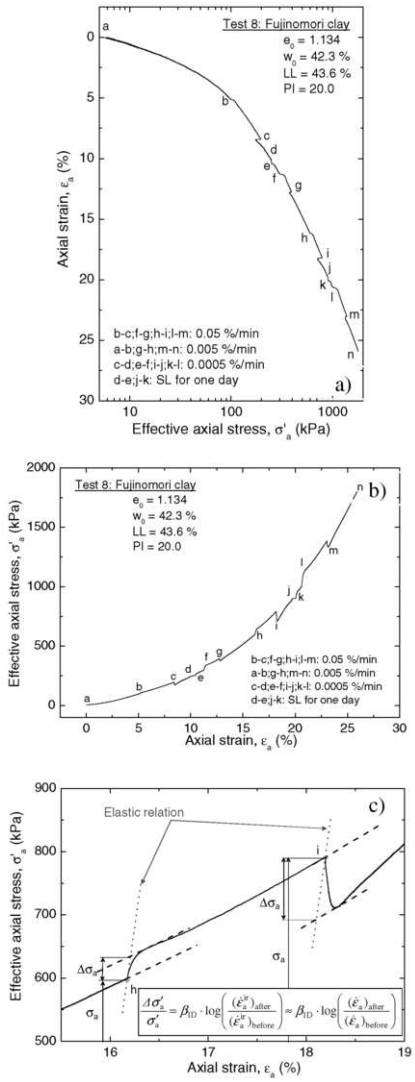

Fig. 4 CRS tests with step changes in the strain rate during primary loading, Fujinomori clay

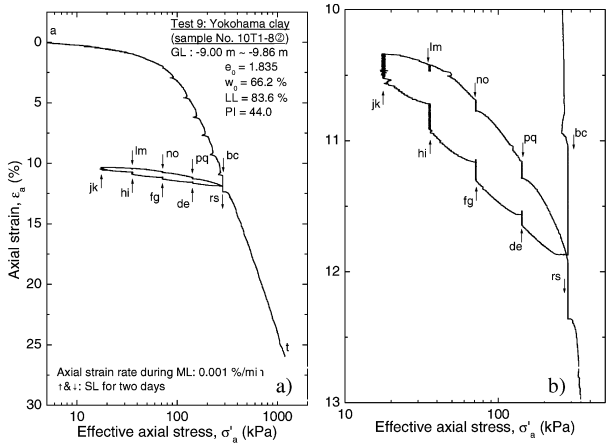

Fig. 5 a) SL during primary loading, unloading and reloading; b) zoom-up of loop in Fig. 5a, Yokohama clay

tests comprising continuous loading, unloading and reloading at different constant axial strain rates, $\dot{\varepsilon}_a$; and 3) special CRS tests including many step changes in $\dot{\varepsilon}_a$ and SL stages.

3 TEST RESULTS

In Fig. 3a, the ε_a - $\log\sigma'_a$ curves from the CRS tests at different $\dot{\varepsilon}_a$ values are noticeably different, while the (ε_a , σ'_a) states after 24 hours at the constant σ_a stages in the SCT, where the $\dot{\varepsilon}_a$ values have become very low, are consistent with these CRS test results. Such *Isotach* viscosity as above is also seen in: 1) test 8 (Fig. 4), where $\dot{\varepsilon}_a$ was changed stepwise many times; and test 5 (Figs. 3b and 6), where reloading was started after having changed the $\dot{\varepsilon}_a$ value. Three broken curves presented in Figs. 4b & 6 denote σ'_a - ε_a relations that are unique for the respective values of $\dot{\varepsilon}_a$.

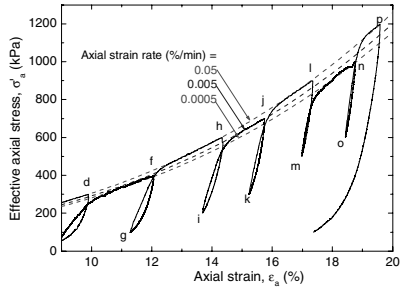

Fig. 6 *Isotach* property in the test depicted in Fig. 3b, Fujinomori clay.

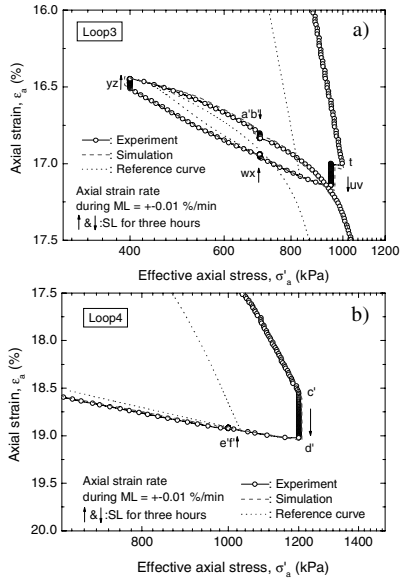

Fig. 7 Loops 3 & 4 in the test depicted in Fig. 3c, Fujinomori clay

Figs. 7a & b show the details of loops 3 & 4 presented in Fig. 3c. Fig. 8 describes creep strains at several SL stages in that test. The simulations of these test results presented in Figs. 7 & 8 are explained later. It may be seen from these figures that the creep strain rate is always positive at the all SL stages starting during 'primary loading' in that σ'_a is increasing at $\dot{\varepsilon}_a > 0$; negative at most SL stages starting during 'unloading' in that σ'_a is decreasing at $\dot{\varepsilon}_a < 0$; and positive again at the all SL stages starting during 'reloading' in that σ'_a is increasing at $\dot{\varepsilon}_a > 0$. These trends can also be seen from Figs. 3d & 5. On the other hand, at SL stage u→v during otherwise 'unloading' in that σ'_a is decreasing at $\dot{\varepsilon}_a < 0$, which is immediately after load reversal from 'primary loading', the creep strain rate is positive (Figs. 8a & 7a). Furthermore, the creep strain rate is kept nearly zero at SL stage e'→f' (Fig. 8b).

All these trends can be interpreted in a unified way by the three-component model (Fig. 1) as follows, noting that $\dot{\varepsilon}_a$ is decomposed into elastic and irreversible components as $\dot{\varepsilon}_a = \dot{\varepsilon}_a^e + \dot{\varepsilon}_a^{ir}$. Fig. 9 illustrates several SL stages during a single global unload/reload cycle at a constant $\dot{\varepsilon}_a$. Then, the following loading definitions become necessary (Tatsuoka et al. 2002). Primary loading is defined as the process where $\dot{\varepsilon}_a^{ir} > 0$ irrespective of previous loading histories and the signs of instantaneous $\dot{\sigma}'_a$ and $\dot{\varepsilon}_a$. The reference curve (R.C.) for primary loading is obtained by primary loading at $\dot{\varepsilon}_a^{ir} = 0$ (with no viscous effect), which is assumed to be in parallel to the primary loading curve at a constant $\dot{\varepsilon}_a$. So, the states between points 1 and 2 are under the primary loading condition despite that $\dot{\sigma}'_a < 0$ and $\dot{\varepsilon}_a < 0$. Then, the creep strain rate is positive at any SL stage between points 1 and 2 (such as SL stages j→k & u→v in Fig. 3c). No creep strain develops when SL starts from point 2, which is the neutral state located on the R.C. for primary loading (such as stage e'→f' in Fig. 3c). Unloading is defined as the process where $\dot{\varepsilon}_a^{ir} < 0$ irrespective of the signs of instantaneous $\dot{\sigma}'_a$ and $\dot{\varepsilon}_a$. In Fig. 9, the R.C. for unloading starts from point 2. During unloading between points 2 and 4, the viscous stress, σ_a^v (Fig. 1), is negative and the creep strain rate is negative at a SL stage (Figs. 7 & 8). Reloading is defined as the process where $\dot{\varepsilon}_a^{ir} > 0$ while before rejoining the primary loading state. The R.C. for reloading starts from point 4 and ends at point 5, where it rejoins the R.C. for primary loading. Both σ_a^v and creep strain rate are positive at a SL stage (Figs. 7 & 8). In the tests performed in this study, the all SL stages during otherwise 'reloading' of σ'_a started with $\dot{\varepsilon}_a^{ir} > 0$.

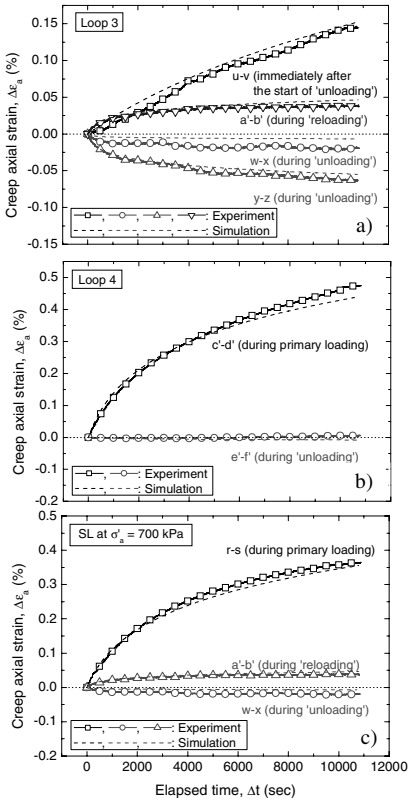

Fig. 8 Time histories of creep strain in the test depicted in Fig. 3c, Fujinomori clay: a) & b) several SL stages in loops 3 & 4; and c) SL at the same σ'_a during primary loading, 'unloading' and 'reloading'.

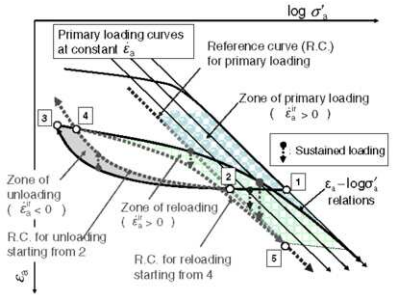

Fig. 9 Reference curves for primary loading, unloading & reloading

Referring to Fig. 4c, the viscous property can be quantified by the changing rate of σ'_a upon a step change in $\dot{\varepsilon}_a$, defined by the equation shown in Fig. 10 (Di Benedetto et al. 2002; Tatsuoka et al. 2002, 2008). The data presented in Fig. 10 are from the test depicted in Fig. 4 and another on Yokohama clay. With both clays, the relation is linear while independent of the values of σ'_a and $\dot{\varepsilon}_a$ at which $\dot{\varepsilon}_a$ is changed stepwise. The slope of the linear relation, β_{1D}, of Yokohama clay is larger, presumably reflecting a higher plasticity index.

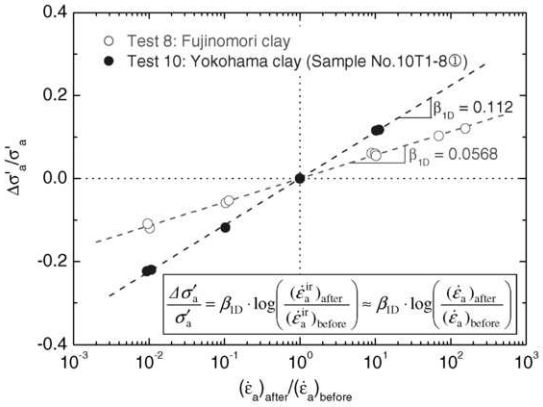

Fig. 10 Rate sensitivity coefficients, β_{1D}

Table 2. Parameters of the viscosity function

Clay type	α	m	$\dot{\varepsilon}_r^{ir}$, %.sec
Fujinomori	0.5	0.05	10^{-8}
Yokohama	1.5	0.045	10^{-7}

4 SIMULATIONS

Simulations of typical tests, presented in Figs. 7 and 8, were performed as follows: 1) The R.C.s for primary loading, unloading and reloading were determined so that the ultimate ends after an infinite period at SL stages are located on the respective R.C.s. In these tests, the hysteresis loops of R.C. relation during an unload/reload cycle are not closed but crossing without returning to the starting point (as illustrated in Fig. 9). This trend becomes stronger with an increase in the irreversible negative axial strain increment during unloading. 2) σ'_a is decomposed into the inviscid and viscous components (Fig. 1). For primary loading, σ'_a is obtained as: $\sigma'_a = \sigma_a^f + \sigma_a^v = \sigma_a^f[1 + g_v(\dot{\varepsilon}_a^{ir})]$, where the σ_a^f - ε_a^{ir} relation is the R.C. relation expressed in terms of ε_a^{ir}; and $g_v(\dot{\varepsilon}_a^{ir})$ is the viscosity function, equal to $\alpha \cdot [1 - \exp\{1 - (|\dot{\varepsilon}^{ir}| / \dot{\varepsilon}_r^{ir} + 1)^m\}]$ (≥ 0). The parameters were determined based on β_{1D} (Table 2). When $\dot{\varepsilon}_a^{ir} = 0$, $g_v(\dot{\varepsilon}_a^{ir}) = 0$ and $\sigma'_a = \sigma_a^f$ (non-zero values, unlike the *Isotach* model proposed by Kim & Leroueil, 2001). This feature is essential to describe the behaviours during global unloading/reloading as well as primary loading. 3) By assuming the same *Isotach* viscosity in the whole process, σ'_a during unloading and reloading are obtained from $\sigma'_a - [\sigma'_a]_{UL} = \{\sigma_a^f - [\sigma_a^f]_{UL}\}[1 - g_v(|\dot{\varepsilon}_a^{ir}|)]$ (unloading), where $|\dot{\varepsilon}_a^{ir}|$ is the absolute value of $\dot{\varepsilon}_a^{ir}$; and $\sigma'_a - [\sigma'_a]_{RL} = \{[\sigma_a^f]_{UL} / ([\sigma_a^f]_{UL} - [\sigma_a^f]_{RL})\} \cdot \{\sigma_a^f - [\sigma_a^f]_{RL}\}[1 + g_v(|\dot{\varepsilon}_a^{ir}|)]$ (reloading). The subscript 'UL' and 'RL' denote respectively the coordinates at load reversing (e.g., points 2 & 4 in Fig. 9). 4) The timings at the start and end of respective primary loading, unloading and reloading regimes as well as SL stages in the simulations follow the respective measured time histories of ε_a. Only the SL stages during unloading were started when the simulated σ'_a value became the measured value. This method was adopted because small errors in the simulated creep strain that have accumulated during the precedent SL stages result in a large error in the simulated σ'_a value due to a high stiffness of clay during unloading. As seen from Figs. 7 and 8, the loading rate effects, including the creep behaviour, observed in the experiments are well simulated.

5 CONCLUSIONS

The following conclusions can be derived:

1) The viscous properties of the two types of clay observed in 1D compression tests were of the *Isotach* type.
2) The loading condition should be defined based on the sign of instantaneous irreversible strain rate. Then, the creep strain rate at sustained loading during otherwise primary loading and reloading is positive while the one during otherwise unloading is negative.
3) The loading rate effects observed under rather general loading conditions can be well simulated by a non-linear three-component elasto-viscoplastic model incorporating different reference curves (without viscous effects) for primary loading, reloading and unloading conditions.

ACKNOWLEDGEMENT

The authors are grateful to the Metropolitan Expressway Co. Ltd. and the OYO Co. Ltd. for providing the undisturbed clay samples.

REFERENCES

Acosta-Martínez H., Tatsuoka, F. & Li Jianghzhong. 2005. Viscous property of clay in 1-D compression: evaluation and modeling. *Proc. 16th ICSMGE*, *Osaka*: 779-783.

Adachi, T., Oka, F. & Mimura, M. 1996. Modeling aspects associated with time dependent behavior of soils. *Measuring and Modeling Time Dependent Soil Behavior*, ASCE GSP 61: 61-95.

Di Benedetto, H., Tatsuoka, F. & Ishihara, M. 2002. Time-dependent deformation characteristics of sand and their constitutive modeling. *Soils and Foundations*, Journal of Japanese Geotechnical Society, Vol.42, No.2: 1-22.

Imai, G. 1995. Analytical examination of the foundations to formulate consolidation phenomena with inherent time-dependence. *Proc. Int. Symp. on Compression and Consolidation of Clayey Soils*, IS Hiroshima '95. (2): 891-935. Rotterdam: Balkema.

Kim, Y.-T. & Leroueil, S. 2001. Modeling the viscoplastic behaviour of clays during consolidation: application to Berthierville clay in both laboratory and field conditions. *Canadian Geotechnical Journal*, 38: 484-497.

Leroueil, S. & Marques, M.E.S. 1996. Importance of strain rate and temperature effects in geotechnical engineering. *Measuring and Modeling Time Dependent Soil Behavior*, ASCE GSP 61: 1-60.

Niemunis, A. & Krieg, S. 1996. Viscous behaviour of soil under oedometric conditions. *Canadian Geotechnical Journal* 33: 159-168.

Tanaka, H. 2005a. Consolidation behaviour of natural soils around p_c value – long term consolidation test -. *Soils and Foundations*, 45(3): 83-95.

Tanaka, H. 2005b. Consolidation behaviour of natural soils around p_c value – inter-connected oedometer test -. *Soils and Foundations*. 45(3): 97-105.

Tatsuoka, F., Ishihara, M., Di Benedetto, H. & Kuwano, R. 2002. Time-dependent deformation characteristics of geomaterials and their simulation. *Soils and Foundations*. 42(2): 103-129.

Tatsuoka, F., Di Benedetto, H., Enomoto, T., Kawabe, S. & Kongkitkul, W. 2008. Various viscosity types of geomaterials in shear and their mathematical expression. *Soils and Foundations*. 48(1): 41-60.